

Common-Mode Impedance of a Ferrite Toroid on a Cable Harness

Natalia Bondarenko^{1, *}, Marina Koledintseva², Peng Shao³, Phil Berger⁴,
David Pommerenke⁴, and Daryl Beetner⁴

Abstract—Ferrite toroids (or clamps) are widely used to reduce common-mode (CM) currents in power systems. The CM impedance of the ferrite depends on the frequency-dispersive permeability and permittivity of the ferrite, the geometry of the system, and the location of the ferrite in it. An analytical model was developed to predict the CM impedance of a wire harness above a return plane with a ferrite on it. The model is based on transmission line theory for a cable, a ferrite, and a return plane. The parameters of the model are calculated using a frequency-dependent quasistatic model for a ferrite toroid. This model accurately predicts the CM impedance of a mock harness within 3 dB up to 1 GHz. The proposed model is also applied to a real power system consisting of an inverter and a motor. Knowledge of the CM impedance of the system in the operating regime is critical to determining the impact of the ferrite on CM currents. The CM impedance is determined using the dual current clamp technique. The impact of the ferrite on the CM impedance and currents of the power inverter system was predicted within 3 dB, demonstrating the usefulness of the modelling approach for analysis of power systems.

1. INTRODUCTION

Ferrite toroids (or clamps) are used to reduce common-mode (CM) currents on cables and wire bundles in power systems by increasing their CM impedance and providing loss over a certain frequency range. A typical power system is shown in Figure 1. It consists of a source (a power inverter), a three-phase power cable over a return plane (a metal chassis), and a load (a motor). The power inverter produces CM current on the power cable, which can generate unwanted radiation. A ferrite toroid can be placed on the power cable to reduce CM current.

The best choice for a ferrite component depends on many factors, including the CM impedance of the system and the toroid. The impedance of a ferrite core, typically a toroidal structure made of non-conducting magneto-dielectric ferrite material, depends on its permittivity and permeability, as well as geometrical factors like the size and shape of the toroid, the geometry of the system the ferrite is used in, and the position of the ferrite core within this system [1–13]. Determining the best toroid through experimental “trial and error”, where multiple ferrite toroids are placed in a system to observe the change in emissions, may be expensive and time-consuming, and often does not yield an optimal solution, particularly when size and weight are a concern.

The objective of this work is to predict the effects of ferrite toroids on the CM impedance and CM current of a power system when the ferrite is placed on the cable harness. Predicting these effects requires a simple analytical or semi-analytical model of a ferrite toroid. Of particular interest is the case where the harness runs above a return plane. A model for the ferrite and harness was built using transmission line theory to account for wave propagation effects through the ferrite, and using

Received 14 July 2018, Accepted 9 September 2018, Scheduled 31 October 2018

* Corresponding author: Natalia Bondarenko (nbcnc@mst.edu).

¹ Cisco Systems, Inc., 375 E Tasman Dr., San Jose, CA, CA 95134, USA. ² Electromagnetic Compatibility Design, Oracle Corp., 4090 Network Cir., Santa Clara, CA 95054, USA. ³ Firefly Dimension, Inc., 3165 Olin Ave, San Jose, CA 95117, USA. ⁴ EMC Lab, Electrical Engineering Department, Missouri University of Science and Technology, Rolla, MO 65401, USA

a frequency-dependent quasistatic model of the ferrite toroid. Since power systems typically generate problematic emissions at frequencies less than 1 GHz (usually up to a few hundreds of MHz), a working bandwidth up to 1 GHz was targeted for the model. Methods were also developed to apply the model within “real” power systems, where the harness CM impedance must be found when the system is turned on and running.

Although there are several publications describing models of ferrite cores [1–5], the simple models are applicable only at relatively low frequencies (less than a hundred MHz). More complex lumped element models for ferrite cores may extend the frequency range [6–8]. In these published works, however, no propagation effects in the extended structures are considered. The radiated electric field from a system of a wire and a ferrite toroid suspended over the return plane is considered in [9] at frequencies up to 1 GHz, but these results are not sufficient to retrieve the CM impedance of power systems of interest. In [10], various techniques to damp electromagnetic interference (EMI) in power systems are overviewed and classified. The frequency-dependent RLC parameters of toroidal and axial inductors with wire windings were considered in [11]. This model was applied to the surface-mounted components on printed circuit boards in [12, 13]. The approach in [11–13] for toroids may be modified and applied to a ferrite toroid on a wire, but only at low frequencies. This was done in [14], where the frequency range was limited to about 200 MHz. No traveling-wave effects were taken into account, however, which limited the applicable frequency range of the published models. In addition, no connectors or supporting planes were considered either. None of the models in the literature fully account for the CM current on the return structure, and there are no simple analytical models to quantify the CM impedance of a power system with a ferrite core. Information about the CM impedance is required to understand the impact of the ferrite.

In this paper, transmission line theory is used with a frequency-dependent quasistatic model of the ferrite toroid to predict the effects of the toroids on the CM loop impedance and CM current of a power system. The CM loop impedance (the term introduced and described in details in [15]) is an impedance looking into a setup that consists of a set of source impedances, single-wire or multi-wire transmission lines, and a set of load impedances. This impedance is not trivial to measure, since a ‘loop’ of an active system cannot always be broken to make this measurement. Additionally, the return path is typically unknown or is embedded in the physical structure. The dual current probe method [15] is one possible approach to non-invasively measure the CM impedance of the system. This method was initially tested to predict the impact of ferrites on a system in [16]. The present paper extends the work in [16] through development of a simple approximate analytical broadband model of the ferrite toroid and through application of the model to analyze a real power inverter/motor system.

The structure of the paper is as follows. The analytic model of a harness with a ferrite toroid over a metal chassis is developed in Section 2, and per-unit-length parameters for the toroid are derived. Section 3 contains an experimental validation of the model in a simple laboratory setup. In Section 4, methods are presented and tested for using the model within a real, active, power inverter system. The conclusions are summarized in Section 5.

2. ANALYTICAL MODEL

The electrical behavior of a ferrite toroid depends not only on the constitutive parameters of the ferrite material, but also on the geometry of the structure where it is employed. The structure used here is shown in Figure 1. The multi-phase power cable is represented by a single wire, since CM currents see this harness as a single conductor. The current return path is represented as a solid perfectly-conducting plane, located underneath the cable. The test structure can thus be treated as a two-conductor distributed transmission line system carrying a single propagating TEM wave. This approximation is most appropriate when the cable or ferrite is electrically long. Higher-order modes may appear at high frequencies, but they are not considered in this model. A simple test structure and the equivalent model of this structure used for initial experiments are shown in Figure 2.

The input impedance seen by the source looking into the cable is needed to characterize the system behavior. The characteristic impedance of a transmission line with a single propagating TEM wave, $Z = \sqrt{(R + j\omega L)/(G + j\omega C)}$, and the propagation constant, $\gamma = \sqrt{(R + j\omega L) \cdot (G + j\omega C)}$, both depend on the per-unit-length RLGC (resistance, inductance, conductance, and capacitance) parameters

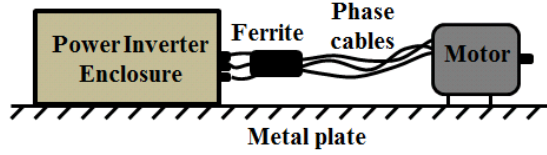


Figure 1. A power system with a power cable bundle using a ferrite core.

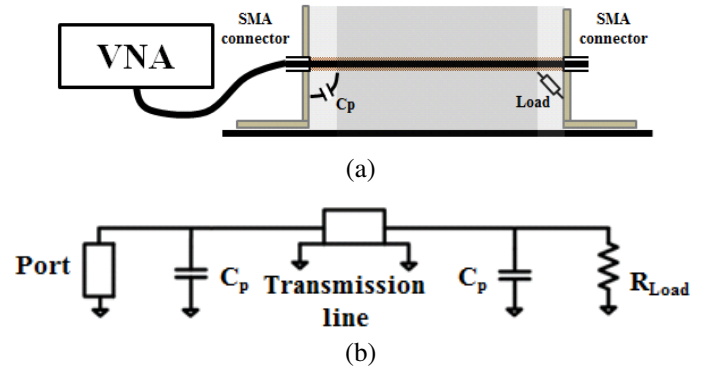


Figure 2. Simplified structure of the system under test: (a) representation of the system as a conductor over a return plane connecting a source and load, and (b) an equivalent circuit for the structure.

for the line. For a lossless transmission line running through the air above a return plane, the RLGC parameters [17] are

$$R = \frac{1}{2\pi r_{wire} \delta \sigma_c}; \quad (1)$$

$$L = \frac{\mu_0}{2\pi} \ln \left(\frac{2h}{r_{wire}} \right); \quad (2)$$

$$C = \frac{2\pi \epsilon_0}{\ln \left(\frac{2h}{r_{wire}} \right)}; \quad (3)$$

$$G = 0, \quad (4)$$

where σ_c is the conductivity, δ the skin depth of the conductor, r_{wire} the radius of the conductor, and h the height of the conductor over the return plane.

Formulas to calculate the RLGC parameters of a cable suspended over a return plane with and without a ferrite toroid are derived below. The ferrite structure is assumed to be concentric, which is the most common practical case, since the ferrite toroid typically tightly embraces the cable for better elimination of the possible surface currents by the magnetic properties of the ferrite. During measurements, supporting styrofoam washers were used to assure the concentric position of the cable and the toroids.

2.1. Calculation of Per-Unit-Length Inductance (L)

The per-unit-length inductance of an infinitely long transmission line is given by

$$L = \frac{\psi}{I \cdot l} = \frac{\int \mathbf{B} \cdot d\mathbf{S}}{I \cdot l}, \quad (5)$$

where \mathbf{B} is the magnetic flux density created by CM current I along the wire, and the integral is performed over an infinitesimally long loop between the wire and the return plane with area $d\mathbf{S}$. ψ is the total flux through the loop, and l is the overall length of the transmission line. Since the loop consists of a conductor over a return plane, the electrical parameters can be found using image theory (Figure 3). The return plane can be removed and replaced with a mirror image of the conductor. The flux penetrating the area between the conductor and the return plane is calculated to obtain the equivalent inductance per-unit-length. The flux is generated by both the CM current and its image. The magnetic flux density is higher in the ferrite material than in air.

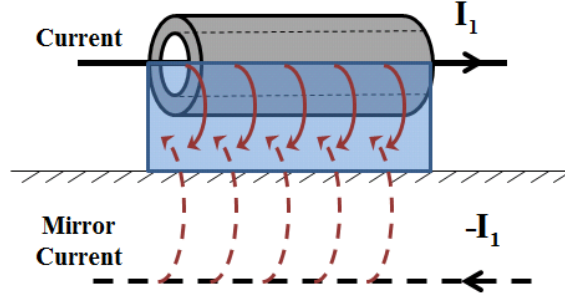


Figure 3. Calculation of the inductance per unit length of the transmission line through the ferrite toroid.

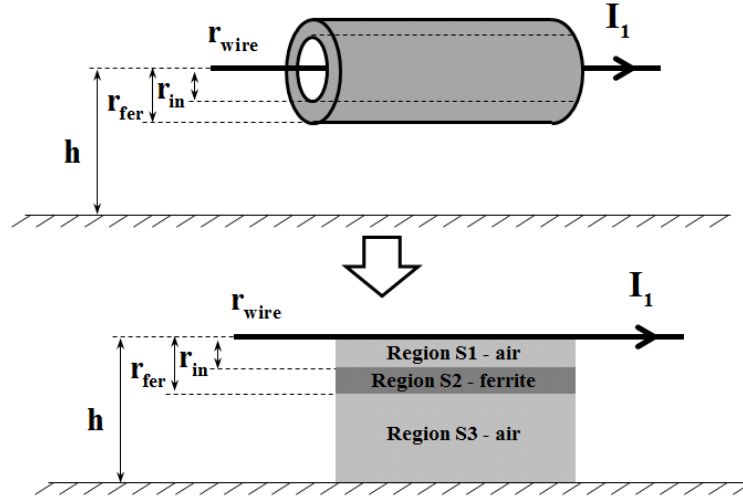


Figure 4. Geometry associated with the ferrite over the return plane.

It is reasonable to assume that the inner radius of the toroid is much less than the height of the cable above the return plane ($r_{in} \ll h$), as is shown in Figure 4. The maximum magnetic flux density in the ferrite generated by the mirror current is given by

$$B_{mirror} = \frac{I\mu}{2\pi(h + h - r_{fer})}, \quad (6)$$

where r_{fer} is the outer radius of the ferrite. The maximum flux density in the ferrite produced by the current on the cable is given by

$$B_c = \frac{I\mu}{2\pi r_{in}}, \quad (7)$$

where r_{in} is the inner radius of the ferrite. Since

$$\frac{I\mu}{2\pi(h + h - r_{fer})} < \frac{I\mu}{2\pi h} \ll \frac{I\mu}{2\pi r_{in}}, \quad (8)$$

the flux generated by the mirror current is negligible and can be ignored.

The magnetic flux between the wire and the return plane was calculated over three regions as shown in Figure 4: S1 is the area between the cable and the ferrite ($\mu = \mu_0$); S2 is the area inside the ferrite ($\mu = \mu_0 \cdot \mu_{r_fer}$), and S3 is the area between the ferrite and the return plane ($\mu = \mu_0$). The magnetic flux per-unit-length within each region is

$$\psi_1 = \int_{S1} \mathbf{B} d\mathbf{S} \approx \int_{r_{wire}}^{r_{in}} \frac{I\mu_0}{2\pi r} dr, \quad (9)$$

$$\psi_2 \approx \int_{r_{in}}^{r_{fer}} \frac{I\mu_0\mu'_r}{2\pi r} dr, \quad (10)$$

and

$$\psi_3 \approx \int_{r_{fer}}^h \frac{I\mu_0}{2\pi r} dr, \quad (11)$$

where ψ_1 , ψ_2 , and ψ_3 are the per-unit-length magnetic flux in regions $S1$, $S2$, and $S3$, respectively, and μ'_r is the relative permeability of the ferrite. Solving Eqs. (9)–(11), the total flux between the wire and the return plane is

$$\psi \approx \frac{\mu_0 I l}{2\pi} \left[\ln \left(\frac{r_{in}}{r_{wire}} \right) + \ln \left(\frac{h}{r_{fer}} \right) + \mu'_{r-fer} \ln \left(\frac{r_{fer}}{r_{in}} \right) \right], \quad (12)$$

and the per-unit-length inductance is

$$L_{fer} = \frac{\mu_0}{2\pi} \left[\ln \left(\frac{r_{in}}{r_{wire}} \right) + \ln \left(\frac{h}{r_{fer}} \right) + \mu'_{r-fer} \ln \left(\frac{r_{fer}}{r_{in}} \right) \right], \quad (13)$$

2.2. Calculation of Per-Unit-Length Resistance (R)

The per-unit-length resistance of the transmission line with the ferrite toroid is due to the skin-effect in the conductor and to the ohmic loss in the ferrite. The magnetic loss in the ferrite toroid is associated with the imaginary part of permeability. By replacing μ'_{r-fer} in Eq. (13) with $\omega\mu''_{r-fer}$ and $\omega\mu''_{r-air}$ for air, where $\omega = 2\pi f$ is the angular frequency, and one can find the per-unit-length resistance associated with the ferrite toroid as

$$R_{fer} \approx \frac{\omega\mu_0}{2\pi} \left[\mu''_{r-air} \ln \left(\frac{r_{in}}{r_{wire}} \right) + \mu''_{r-air} \ln \left(\frac{h}{r_{fer}} \right) + \mu''_{r-fer} \ln \left(\frac{r_{fer}}{r_{in}} \right) \right]. \quad (14)$$

Since there is practically no magnetic loss in the air, the per-unit-length resistance due to the ferrite toroid is then

$$R_{fer} = \frac{\omega}{2\pi} \mu_0 \mu''_{r-fer} \ln \left(\frac{r_{fer}}{r_{in}} \right). \quad (15)$$

These losses will dominate conductive losses over the frequencies where the ferrite is used.

2.3. Calculation of Per-Unit-Length Capacitance (C)

The electric field distribution between the wire and return plane is affected by the presence of the ferrite toroid. Analytical calculation of the capacitance requires simplifying assumptions. For this purpose, the electric field between the conductor and the ferrite, and the electric field within the ferrite are assumed to be radially symmetric.

The cross-section of the cable and ferrite over the ground plane with the corresponding parts of the capacitance are shown in Figure 5.

The per-unit-length capacitance between the conductor and the ferrite, C_1 , and the per-unit-length capacitance between the inner and outer surface of the ferrite, C_2 , can be calculated from the capacitance of the coaxial structure as

$$C_1 \approx \frac{2\pi\epsilon_0}{\ln \left(\frac{r_{in}}{r_{wire}} \right)} \quad (16)$$

and

$$C_2 \approx \frac{2\pi\epsilon_0\epsilon'_r}{\ln \left(\frac{r_{fer}}{r_{in}} \right)}, \quad (17)$$

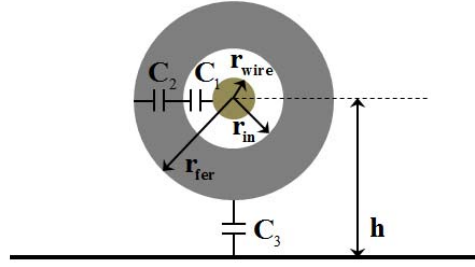


Figure 5. Cross-section of the cable and ferrite over the return plane.

where ε'_r is the real part of permittivity of the ferrite. The per-unit-length capacitance between the ferrite and the return plane, C_3 , can be found from the formula for capacitance of a conductor over a return plane

$$C_3 = \frac{2\pi\varepsilon_0}{\cosh^{-1}\left(\frac{h}{r_{fer}}\right)}. \quad (18)$$

The total per-unit-length capacitance of the ferrite part is found from the three capacitors in series,

$$C_{fer} = \frac{1}{\frac{1}{C_1} + \frac{1}{C_2} + \frac{1}{C_3}}. \quad (19)$$

2.4. Calculation of Per-Unit-Length Conductance (G)

The per-unit-length conductance of a ferrite toroid can be found from the capacitance associated with the ferrite and the dielectric loss in the ferrite as [18]

$$G_{fer} = \omega C_2 \frac{\varepsilon''_r}{\varepsilon'_r}. \quad (20)$$

The RLGC parameters in Eqs. (13), (15), (19), and (20) can be used to find the characteristic impedance and propagation constant for the transmission line including the ferrite. In the next section, this model of the ferrite toroid is validated along with a model of the test structure.

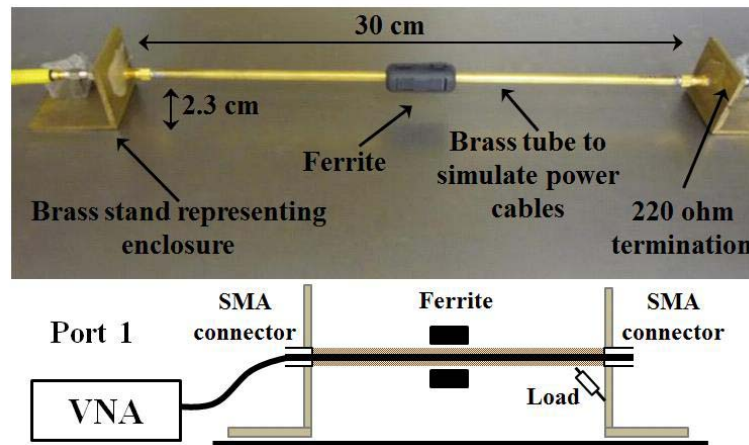


Figure 6. Simplified test structure used to model a real power system.

3. EXPERIMENTAL VALIDATION OF ANALYTICAL MODEL

To validate the approximate analytical model of the ferrite toroid, tests were performed on a simple setup consisting of a brass tube over a return plane as shown in Figure 6. This test setup is analogous to the system shown in Figure 2. Since the details of the test setup are known, the system impedance can be calculated analytically. In the experiment, a Vector Network Analyzer (VNA) was used to measure Z_{11} from the source side of the system, as indicated in Figure 6. Measurements of the input impedance were made both with and without a ferrite placed on the brass tube. In many power systems, the inverter and motor are covered by metal enclosures. In the test setup used here, the enclosure was simulated using L-shaped brass stands, which support the brass tube at a chosen height above the return plane, as is shown in Figure 6. The interface between the brass stand and brass tube creates parasitic capacitances similar to the capacitances that would be seen in a real system with an enclosure. The L-shaped stands are built to have a good electric contact with the return plane. In a real system, the ferrite toroid will be placed around the whole bundle of cables. In the test setup, the ferrite is placed on the brass tube simulating the CM component of current on the cables. The input impedance of the setup calculated analytically will be compared to the measured impedance.

3.1. Test Structure Modeling

The test structure shown in Figures 2 and 6 includes an impedance related to the source, an impedance of the load, a transmission line, and a set of parasitic capacitances between the transmission line and the “enclosure” (the L-shaped brass stands). The source impedance is $50\ \Omega$ and is associated with the VNA. The brass tube over the return plane represents the transmission line. The brass tube was terminated with the brass stand on the right using a $220\ \Omega$ resistor. This termination impedance ($220\ \Omega$) was chosen to approximately match the characteristic impedance of the transmission line when no ferrite was placed on the brass tube.

Lumped element parasitic capacitors, C_p , between the brass tube and brass stands were added to each end of the transmission line to model the parasitic capacitance between the enclosure and brass tube. These capacitors are crucial to an accurate modeling of the high-frequency impedance of the system. They are present at both the source and the load ends of the transmission line. Their values are approximately the same due to the structure symmetry. The value of these capacitors can be derived from the geometry decomposition of the structure around the brass stands, as is shown in Figure 7. The parallel capacitors C' , C'' , and C''' determine the value of C_p in Figure 2(b) as,

$$C_p = C' + C'' + C''', \quad (21)$$

where C' is the capacitance between the brass tube and the brass stand. C'' is the capacitance between the outer shield of the connector and the brass stand, and C''' is the capacitance between the inner conductor of the connector and the brass stand.

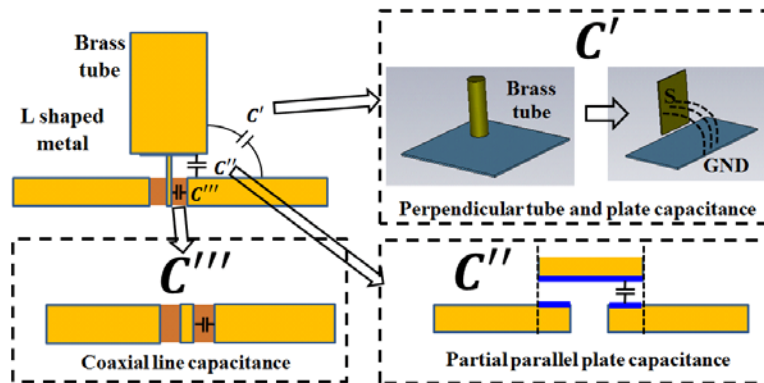


Figure 7. Calculation of capacitance between the brass tube (common-mode carrying conductor) and the brass stand (“enclosure”).

The capacitance C' between the brass tube and the brass stand can be calculated as follows. While the entire brass tube and brass stand contribute to this capacitance, the most important contributors are the portions of the two structures which are closest to each other. The capacitance C' was calculated between a metal plate having the size of the brass stand and a cylindrical conductor with the same length as the height of the brass stand. This capacitance can be approximately estimated by unfolding the cylindrical brass tube into a sheet and then calculating the capacitance between the two perpendicular sheets as [19]

$$C' = \varepsilon_0 \left(\frac{K'(k_{in})}{K(k_{in})} + \frac{K'(k_{out})}{K(k_{out})} \right), \quad (22)$$

where ε_0 is the permittivity of free space, and k_{in} , k_{out} , $K'(\cdot)$, and $K(\cdot)$ are given in [19].

The parameter C'' is the capacitance between the end of the brass tube and the brass stand. This capacitance can be calculated from the capacitance of two parallel plates as is shown in Figure 7:

$$C'' \approx \frac{\varepsilon_0 A}{d}, \quad (23)$$

where A is the area of the end-plate, and d is the distance between the connector and the brass stand.

The capacitance C''' is between the inner conductor and the brass stand over the area where the conductor penetrates the stand, as shown in Figure 7. If fringing fields are neglected, this capacitance can be found from the equation for capacitance of a coaxial structure:

$$C''' \approx \frac{2\pi\varepsilon_0\varepsilon_r}{\ln\left(\frac{r_{inner}}{r_{stand}}\right)}, \quad (24)$$

where r_{inner} is the radius of the inner conductor of the connector; r_{stand} is the inner radius of the hole in the brass stand; in this case, ε_r is the dielectric constant for the standard SMA connector dielectric material (PTFE).

3.2. Impedance of Test Structure without Ferrite

The characteristic impedance of the transmission line without ferrite is calculated using the per-unit-length RLGC parameters. The input impedance at the source end can be calculated step by step starting from the termination ($220\ \Omega$ load) as illustrated in Figure 8. The impedance looking into the load is given by

$$Z_{input_load} = \frac{R_{load}}{R_{load}j\omega C_p + 1}, \quad (25)$$

where R_{load} is $220\ \Omega$ for this setup, and C_p is the capacitance between the brass tube and the brass stand as calculated in the previous section. The input impedance looking into the transmission line after the parasitic capacitance is

$$Z_{input_after_Cp} = Z_0 \frac{Z_{input_load} + Z_0 \tanh(\gamma l)}{Z_0 + Z_{input_load} \tanh(\gamma l)}, \quad (26)$$

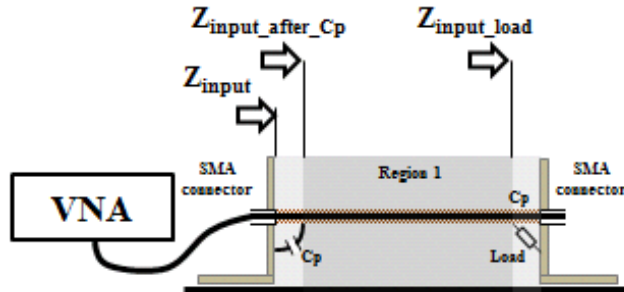


Figure 8. Distinguishing input impedances of the structure.

where $Z_0 = \sqrt{\frac{R_0 + j\omega L_0}{G_0 + j\omega C_0}}$ is the characteristic impedance of region 1 in Figure 8; R_0, L_0, G_0 and C_0 can be found as in Eqs. (1)–(4); l is the length of region 1. The impedance looking into the transmission line from the source Z_{input} is

$$Z_{input} = \frac{Z_{input_after_Cp}}{Z_{input_after_Cp} j\omega C_p + 1}, \quad (27)$$

The input impedance, $Z_{11} = Z_{input}$, was calculated analytically and measured using a VNA. The radius of the brass tube used in the experiment was 2.16 mm, and its total length was 30 cm. The distance between the lower points on the brass tube and the return plane was 2.3 cm. The calculated and measured amplitudes and phases of Z_{11} are shown in Figure 9. The measured input impedance and the analytical results agree within less than about 2 dB and 10 degrees up to 1 GHz.

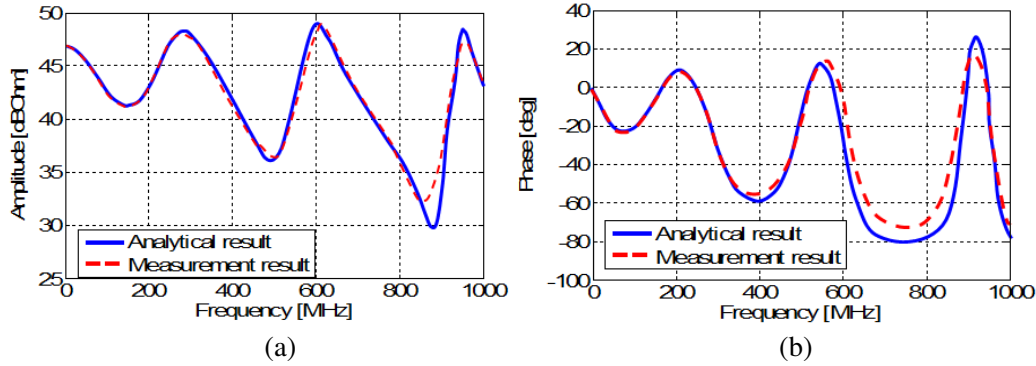


Figure 9. Magnitude (a) and phase (b) of the measured and estimated input impedance of the test structure without a ferrite.

3.3. Test Structure Impedance Including Ferrite Toroid

The next step was to develop and verify a model of the system including a ferrite toroid. The input impedance was calculated using the model shown in Figure 10. The characteristic impedance of the portion of the transmission line containing the ferrite toroid (Region 2 in Figure 10) was found using its RLGC parameters as derived in Section 2.

The impedance looking from the ferrite toward the load is

$$Z_{input_after_ferrite} = Z_0 \frac{Z_{input_load} + Z_0 \tanh(\gamma l_1)}{Z_0 + Z_{input_load} \tanh(\gamma l_1)}, \quad (28)$$

where Z_0 is the characteristic impedance of Region 1; γ is the complex propagation constant in Region 1; R_0, L_0, G_0 and C_0 are obtained from Eqs. (1)–(4); l_1 is the length of Region 1. The impedance looking into the ferrite toward the load is

$$Z_{input_before_ferrite} = Z_{ferrite} \frac{Z_{input_after_ferrite} + Z_{ferrite} \tanh(\gamma_{fer} l_2)}{Z_{ferrite} + Z_{input_after_ferrite} \tanh(\gamma_{fer} l_2)}, \quad (29)$$

where $Z_{ferrite}$ is the characteristic impedance of Region 2, l_2 the length of the ferrite, and γ_{fer} the complex propagation constant in ferrite. $Z_{ferrite}$ is given by

$$Z_{ferrite} = \sqrt{\frac{R_{fer} + j\omega L_{fer}}{G_{fer} + j\omega C_{fer}}}, \quad (30)$$

where $L_{fer}, R_{fer}, C_{fer}, G_{fer}$ can be calculated from Eqs. (13), (15), (19), and (20). The impedance looking into the transmission line from the source end is given by

$$Z_{input_after_Cp} = Z_0 \frac{Z_{input_before_ferrite} + Z_0 \tanh(\gamma l_3)}{Z_0 + Z_{input_before_ferrite} \tanh(\gamma l_3)}, \quad (31)$$

where l_3 is the length of Region 3. The overall input impedance, Z_{input} , is then

$$Z_{input} = \frac{Z_{input_after_Cp_f}}{Z_{input_after_Cp_f} j\omega C_p + 1}, \quad (32)$$

where $Z_{input_after_Cp_f}$ is the input impedance looking into the transmission line after the parasitic capacitance.

The model was tested with a ferrite toroid placed at different locations on the brass tube. The inner radius of the ferrite toroid was 1.2 cm; its outer radius was 1.8 cm; its length was 1.3 cm. The permeability and permittivity of the ferrite material of the toroid are shown in Figure 11. The height of the brass tube above the return plane was 2.3 cm in initial tests. The input impedance was measured and calculated analytically, and the results were compared.

The magnitude and phase of the measured and calculated input impedances are shown in Figure 12 when the ferrite was next to the source (enclosure). The measured and estimated input impedances when the ferrite was placed in the middle of the tube between the two brass plates are shown in Figure 13. Figure 14 shows the measured and estimated input impedance when the height of the cable (the distance between the lower line of the brass tube and the return plane) was doubled to 7.7 cm and the

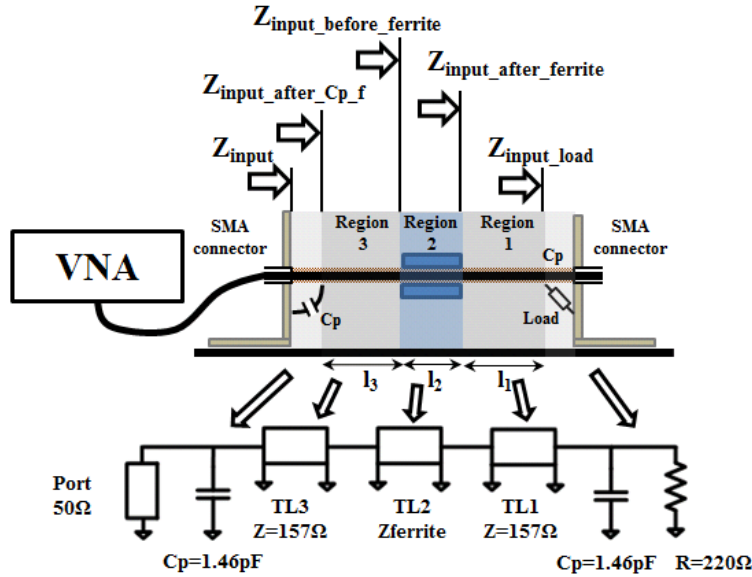


Figure 10. Calculation of input impedance with ferrite on transmission line.

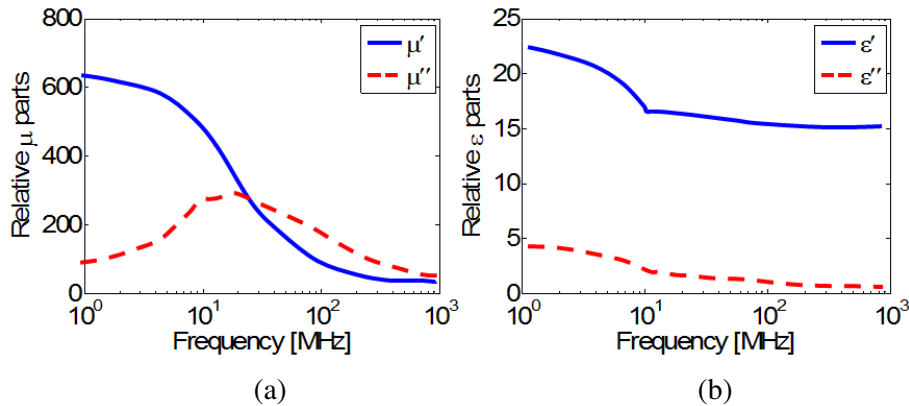


Figure 11. Measured permeability (a) and permittivity (b) of the ferrite toroid.

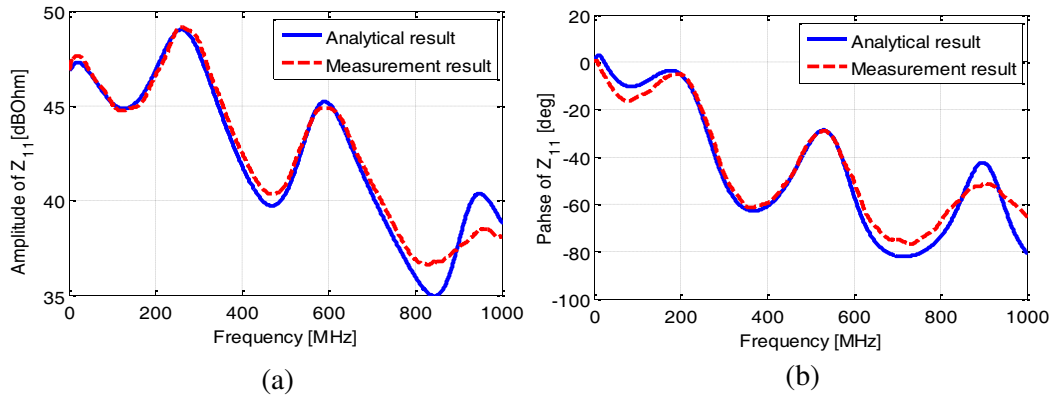







Figure 12. Magnitude (a) and phase (b) of the measured and estimated input impedance of the test structure when the ferrite was placed close to the source.

ferrite was placed next to the source. The measured and calculated impedances match within 2–3 dB up to 1 GHz in all cases.

Ferrite toroids of different sizes and of different compositions were also tested. The dimensions (in mm) of the tested ferrites are indicated in Table 1. Previous tests were performed using ferrite toroid “d”, whose material characteristics are given in Figure 11. Ferrite toroid “e” was made of a different material than ferrites *a–d*. This ferrite had a center frequency of approximately 80 MHz. Measured and simulated impedances matched within 2–3 dB up to 1 GHz. Analysis of the results using Feature Selective Validation (FSV) [20,21], showed that all of the simulated impedances were “good” (max Global Difference Measure = 0.37) to “excellent” (min Global Difference Measure = 0.09).

Table 1. Ferrite toroids under test (all dimensions are in mm).

				
Ferrite a	Ferrite b	Ferrite c	Ferrite d	Ferrite e
$r_{in} = 13.5$	$r_{in} = 8.6$	$r_{in} = 10.3$	$r_{in} = 12$	$r_{in} = 12.7$
$r_{out} = 25.4$	$r_{out} = 19.5$	$r_{out} = 15.9$	$r_{out} = 18$	$r_{out} = 25.6$
$l = 29$	$l = 21.9$	$l = 21.9$	$l = 13$	$l = 39.7$

4. APPLICATION TO A REAL POWER SYSTEM

To apply the ferrite model to a real system requires knowledge of the CM loop impedance of the system. This CM loop impedance, as described in [15], is not trivial to measure. It is often associated with a harness consisting of many conductors, largely depends on parasitics that are unknown and change when the system is active, and also because for an active system a “loop” cannot be broken to make the CM impedance measurement. In this work, the CM loop impedance was measured using the dual

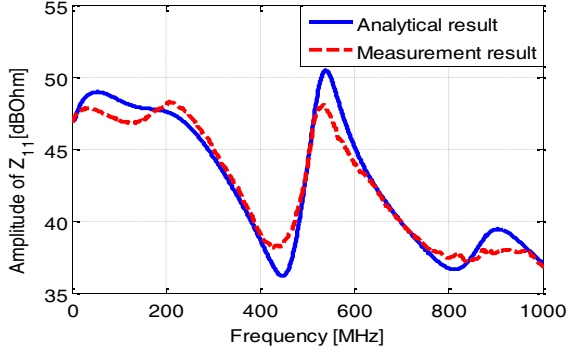


Figure 13. Magnitude of the measured and estimated input impedance of the test structure when the ferrite was placed at the center of the brass tube.

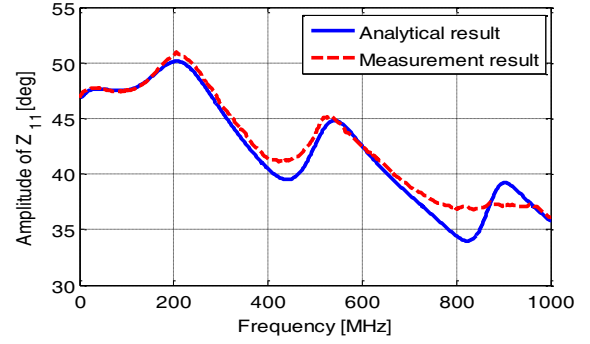


Figure 14. Magnitude of the measured and estimated input impedance of the test structure when the ferrite was placed at a height of 7.7 cm and close to the source.

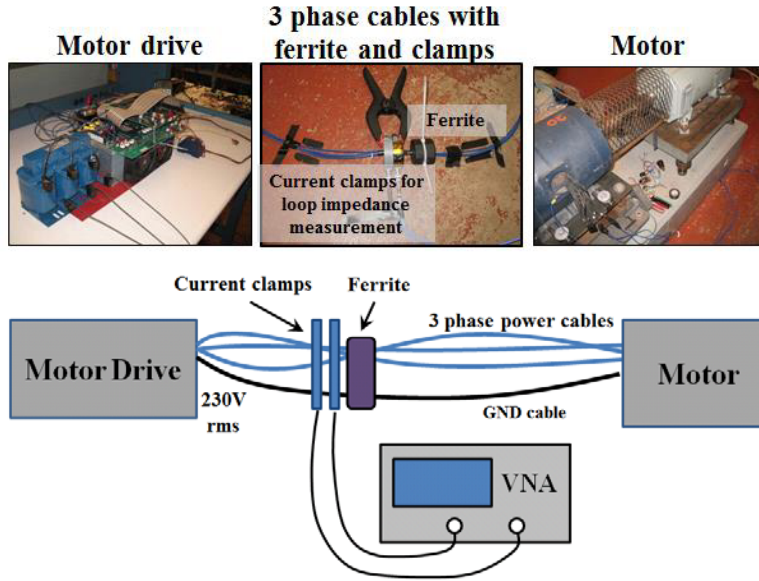


Figure 15. Power system measurement setup.

current probe (DCP) techniques described in [15] and [16]. In this technique, CM energy is injected into the system by one current probe and the resulting CM current is measured by another current probe using a VNA. The CM loop impedance can be found from the amount of injected current. The frequency response of the current probes is de-embedded through a comparatively simple calibration procedure using a special calibration fixture as described in [15, 16].

The ferrite model was tested with a real active power inverter/motor system with emissions up to about 100 MHz. Although the proposed ferrite model agrees well with measurement up to 1 GHz on a mock harness, application to the real system was performed only up to 100 MHz due to the limitations of DCP technique. To predict an influence of a ferrite, the CM circuit of the system was simplified as a CM voltage source in series with a CM loop impedance. Assuming that the ferrite is electrically small below 100 MHz, the CM impedance at the ferrite location can be found as a sum of the original system loop impedance and the analytically calculated ferrite impedance. The CM currents after adding a ferrite is then

$$I_{CM,estimated} = I_{CM,measured} \frac{Z_{CM,loop,measured}}{Z_{CM,loop,measured} + Z_{ferrite,analytical}}, \quad (33)$$

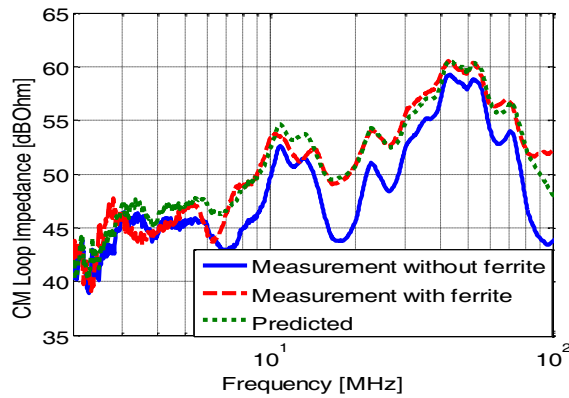


Figure 16. Measured and predicted CM loop impedance with an added ferrite.

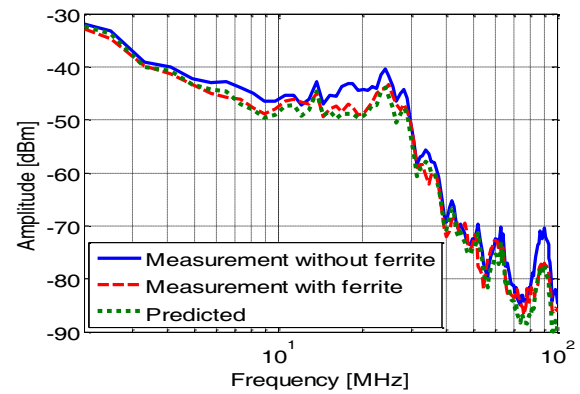


Figure 17. Measured and predicted CM current with an added ferrite.

where $I_{CM,measured}$ and $Z_{CMloop,measured}$ are the measured CM current and CM loop impedance of the ferrite, respectively, and $Z_{ferrite,analytical}$ is the analytically estimated impedance of the ferrite.

The tested power system consists of a motor drive generating 230 V RMS signals, a harness, and a 20 hp motor as shown in Figure 15. A broadband ferrite was placed on the harness as shown in the figure. The CM loop impedance and CM current was measured with and without a ferrite using a VNA. For emissions measurements, the VNA was replaced with a spectrum analyser. The current clamps were placed around all three phase cables.

The measured and predicted CM loop impedances and CM currents with and without a ferrite are shown in Figures 16 and 17. The CM loop impedance and CM current with the ferrite were predicted based on measurements without the ferrite. The proposed model predicted the CM impedance or CM current with the ferrite within 3 dB up to 100 MHz, validating the usefulness of both the ferrite model and the system characterization technique for predicting the impact of ferrites in real power systems. Though the frequency range in this practical example was up to 100 MHz, the proposed model can be applied to the higher frequencies up to 1 GHz.

5. CONCLUSIONS

A comparatively simple analytical model was proposed for a ferrite toroid on a cable above a return plane. This model uses a transmission line description of the cable, ferrite, and return plane, and uses a frequency-dependent, quasistatic approximation of the ferrite to determine transmission line parameters. The proposed model allows prediction of the CM input impedance of a cable with a ferrite toroid on it. Because the model is relatively simple, it provides the possibility of analytically optimizing ferrite characteristics to mitigate unwanted emissions. Efficient variation of ferrite material parameters, toroid and cable geometry, and their placement with respect to the source and to the return plane can be done. Experimental validation of the model showed that the CM impedance of a transmission line with the ferrite could be approximated within 3 dB up to 1 GHz.

The proposed model was further applied to predict the impact of a ferrite on the CM impedance and CM currents of a power system consisting of a power inverter and motor. Measurement of the CM impedance of the system without the ferrite was critical for predicting the impact of the ferrite on the CM current in the active inverter system. This CM loop impedance was determined using the dual current probe approach. Using this impedance as a starting point, the impact of the ferrite on the CM impedance and current was predicted within 3 dB up to 100 MHz (the practical limit of the current clamps and calibration technique). This result demonstrates that the proposed techniques can be useful for applications to power systems.

One possible limitation of the model is that it assumes only TEM propagation through the ferrite above a return plane. If there are not many structures around the power cable, the CM current return path is typically a return plane and, if the return plane is close and frequencies are sufficiently low, the

TEM approximation should be valid. If the CM current does not return through a plane, however, the RLGC model calculated here may not apply. At sufficiently high frequencies, the TEM assumption also breaks down. For the geometry under consideration, the TEM approximation is valid up to 1 GHz. The limiting frequency, however, depends on the geometry of the structure.

ACKNOWLEDGMENT

This work was partially funded through NSF grant IIP-1440110. The authors would also like to thank Laird Technologies and Dr. Yongxue He for providing ferrites toroids for this study.

REFERENCES

1. Izydorczyk, J., "Simulation of ferrites by SPICE," *Proceedings of European Conference on Circuit, Theory and Design*, I/43-I/46, ECCTD05, Cork Ireland, Aug. 29–Sep. 2, 2005.
2. Mohri, K., T. Kohzawa, K. Kawashima, H. Yoshida, and L. V. Panina, "Magneto-inductive effect (MI effect) in amorphous wires," *IEEE Trans. Magnetics*, Vol. 28, No. 5, 3150–3152, Sep. 1992.
3. Muyschondt, G. P. and W. M. Portnoy, "Development of high frequency spice models for ferrite core inductors and transformers," *Industry Applications Conference*, 1328–1333, San Diego, CA, Oct. 1–5, 1989.
4. Yu, Q., T. W. Holmes, and K. Naishadham, "RF equivalent circuit modeling of ferrite-core inductors and characterization of core materials," *IEEE Trans. Electromagn. Compat.*, Vol. 44, No. 1, 258–262, Feb. 2002.
5. Kazimierczuk, M., G. Sancineto, G. Grandi, U. Reggiani, and A. Massarini, "High-frequency small-signal model of ferrite core inductors," *IEEE Trans. Magnetics*, Vol. 35, No. 5, 4185–4191, Sep. 1999.
6. Fujiwara, O. and T. Ichikawa, "An analysis of load effects produced by ferrite core attachment," *Electronics and Communications in Japan*, Part 1, Vol. 80, No. 9, 19–24, 1997.
7. Samir, A. Z. and O. Fujiwara, "Measurement and verification of complex permeability of ferrite material by *S*-parameter techniques," *IEEE Trans. Japan*, Vol. 119-C, 9–14, 1999.
8. Ichikawa, T., H. Kawada, and O. Fujiwara, "An analysis of normal-mode noise caused by braided shield current flowing on coaxial cable attached by a ferrite core," *Trans. IEICE*, Vol. J81-B-II, 327–335, 1998.
9. Maekawa, T. and O. Fujiwara, "Calculation of electric far field radiated from transmission line attached to a ferrite core above a ground plane," *Electronics and Communications in Japan*, Part 1, Vol. 86, No. 5, 2003, Translated from Denshi Joho Tsushin Gakkai Ronbunshi, Vol. J84-B, No. 12, 2374–2381, Dec. 2001.
10. Yazdani, M. R., H. Farzanehfard, and J. Faiz, "Classification and comparison of emi mitigation techniques in switching power converters — A review," *Journal of Power Electronics*, Vol. 11, No. 5, 765–777, Sep. 2011.
11. Naishadham, K., "Closed-form design formulas for the equivalent circuit characterization of ferrite inductors," *IEEE Trans. Electromagn. Compat.*, Vol. 53, No. 4, 923–932, Nov. 2011.
12. Naishadham, K., "Extrinsic equivalent circuit modeling of SMD inductors for printed circuit applications," *IEEE Trans. Electromagn. Compat.*, Special Issue on Printed Circuit Board EMC, Vol. 43, No. 4, 557–565, Nov. 2001.
13. Naishadham, K. and T. Durak, "Measurement-based closed-form modeling of surface-mounted RF components," *IEEE Trans. Microw. Theory Techn.*, Vol. 50, No. 10, 2276–2286, Oct. 2002.
14. Orlando, A., M. Y. Koledintseva, D. G. Beetner, P. Shao, and P. H. Berger, "Lumped-element circuit model of ferrite chokes," *IEEE Symp. Electromag. Compat.*, 754–759, Fort Lauderdale, FL, Jul. 25–30, 2010.
15. Liu, G., Y. Ding, C. Chen, R. Kautz, J. L. Drewniak, D. J. Pommerenke, and M. Y. Koledintseva, "A dual-current-probe method for characterizing CM loop impedance," *IEEE Instrum. Measur. Techn. Conf. (IMTC)*, 1239–1244, Vail, CO, USA, May 2003.

16. Bondarenko, N., P. Shao, M. Koledintseva, D. Beetner, and P. Berger, "Prediction of common-mode current reduction using ferrites in systems with cable harnesses," *Proceeding of IEEE EMC Symposium 2012*, 80–84, Pittsburgh, Aug. 2012.
17. Pozar, D. M., *Microwave Engineering*, Section 2.1, 62, Wiley, 1998.
18. Xu, J., M. Y. Koledintseva, Y. Zhang, Y. He, B. Matlin, R. E. DuBroff, J. L. Drewniak, and J. Zhang, "Complex permittivity and permeability measurements and finite-difference time-domain simulation of ferrite materials," *IEEE Trans. Electromagn. Compat.*, Vol. 52, No. 4, 878–887, Nov. 2010.
19. Xiang, Y., "The electrostatic capacitance of an inclined plate capacitor," *J. Electrostat.*, Vol. 64, 29–34, 2006.
20. *Standard P1597, Standard for Validation of Computational Electromagnetics Computer Modeling and Simulation — Part 1*, 2008.
21. Duffy, A. P., J. M. Martin, A. Orlandi, G. Antonini, T. M. Benson, and M. S. Woolfson, "Feature Selective Validation (FSV) for validation of computational electromagnetic (CEM). Part I — The FSV method," *IEEE Trans. Electromagn. Compat.*, Vol. 48, No. 3, 449–459, Aug. 2006.